Surfaces and Interfaces 44 (2024) 103743

Contents lists available at ScienceDirect

Surfaces and Interfaces

journal homepage: www.sciencedirect.com/journal/surfaces-and-interfaces

A multilayered antifouling coating constructed using the synthesized capsaicin-mimicking N-(4-hydroxy-3-methoxy-benzyl) acrylamide

Hao Yang [a,b], Yi Liu [a], Hidetoshi Saitoh [c], Hao Chen [b,*], Hua Li [a,*]

[a] Zhejing-Japan Joint Laboratory for Antibacterial and Antifouling Technology, Zhejiang Engineering Research Center for Biomedical Materials, Cixi Institute of Biomedical Engineering, Ningbo Institute of Materials Technology and Engineering, Chinese Academy of Sciences, Ningbo 315201, China
[b] Department of Mechanical, Materials and Manufacturing Engineering, University of Nottingham Ningbo China, Ningbo 315100, China
[c] Department of Materials Science and Technology, Graduate School of Engineering, Nagaoka University of Technology, 1603-1 Kamitomioka-machi, Nagaoka, Niigata 940-2188, Japan

ARTICLE INFO

Keywords:
Superhydrophobic coating
Capsaicin-mimicking N-(4-hydroxy-3-methoxy-benzyl) acrylamide
Antifouling activity
Anti-corrosion performance

ABSTRACT

Biofouling is a stepwise accumulation process involving participation of various molecules and marine organisms. To tackle this complex threat, development of efficient long-term antifouling coatings yet keeps elusive. Here we report a newly constructed coating with both antifouling activity and low surface energy. The special surface structure formed by silica spheres and fluorosilanes offers the coating superhydrophobicity. Capsaicin-mimicking N-(4-hydroxy-3-methoxy-benzyl)-acrylamide (HMBA) powder is synthesized via the Friedel-Crafts reaction and is used as the antifoulant additives in the coating. By the synergistic effect of surface superhydrophobicity and the dispersed antifoulant, the multilayered HMBA-silica coating effectively inhibits the adhesion of alginate, bovine serum albumin and *Chlorella*, their adhesion rate on the HS-3 coating is 11.9 %, 8.7 % and 3.3 % respectively. The HS-3 coating kills 96.6 % gram-negative bacteria *E. coli* and 99.9 % gram-positive bacteria *S. aureus*. Furthermore, the HMBA-silica coating significantly mitigates by its superhydrophobicity the corrosion of artificial seawater, its corrosion current density has decreased by 4 orders of magnitude compared to bare 316 L plate. In a 90 days real seawater immersion experiment, the coating shows excellent anti-fouling and anti-corrosion properties. The fabrication route of the HMBA-silica coating using the synthesized broad-spectrum antifoulant HMBA and hydrophobic silica would give insight into developing new antifouling materials for marine applications.

1. Introduction

Biofouling is a persisting complex phenomenon triggered by the undesired accumulation of a variety of molecules, microorganisms, plants, and animals on submerged surface in the marine environment [1]. It is one of the most serious problems in the marine industry since fouling species grown on marine infrastructures usually accelerate the occurrence of corrosion [2]. In addition, the colonized species on the surface cause increase in the weight of ships, resulting in increased fuel consumption and sailing time [3,4]. Furthermore, non-native marine life can be carried into other sea area by colonized marine vessels, leading to bio-invasion [5]. Among the antifouling strategies, depositing an antifouling surface layer has been the predominant approach that has long been proven effective in combating marine biofouling [6,7]. Traditional antifouling coatings usually utilized toxic compounds such as copper, arsenic and tributyltin (TBT) [8]. However, due to the non-selective and long-lasting toxicity of these coatings, a huge threat was posed to all marine life as well as humans [9]. With the banned use of TBT by the International Marine Organization in 2008 and the strictly restricted use of heavy metal-based antifouling agents, there is an urgent need to develop environmentally friendly and multifunctional antifouling coatings [1,10].

In nature, lotus leaves have excellent low surface energy that plays a major role in giving rise to self-cleaning properties [11,12]. The special villi structure and the tiny waxy particles on the surface of lotus leaves could capture air and form a physical barrier [13]. Lotus leaves were found in the Cassie-Baxter wettability state and exhibited superhydrophobicity [14]. Inspired by the special characteristics of micro-nano topographical structure and low surface energy, many superhydrophobic coatings with water contact angle of larger than 150°

* Corresponding authors.
E-mail addresses: hao.chen@nottingham.edu.cn (H. Chen), lihua@nimte.ac.cn (H. Li).

https://doi.org/10.1016/j.surfin.2023.103743
Received 2 September 2023; Received in revised form 15 November 2023; Accepted 10 December 2023
Available online 12 December 2023

and sliding angle of less than 10° have been developed and applied for anti-icing [15], anti-fog [16], oil-water separation [17], corrosion resistance [18,19], and water harvesting [20], etc. Zhang et al. [21] fabricated a skin-inspired triple-layered epoxy-based superhydrophobic coating through a facile spraying process. The coating can provide sustained liquid repellency, anticorrosion, and flame retardancy even under harsh environments. Li et al. [22] dip-coated an antibacterial and superhydrophobic coating on cotton fabrics. High contact angle above 155°, good flame retardancy and appreciable antibacterial performance was reported, which was believed to be due to the presence of quaternary ammonium and alkyl chain structures of the coating. Zhang et al. [18] proposed a manganese stearate superhydrophobic coating via one-step electrodeposition strategy. It was found that the coating with high water contact angle (169.7°) could effectively delay the occurrence of corrosion by reducing the corrosion current density more than 4 orders of magnitude compared to the substrate and suppressing biofouling induced by algae. Long-chain perfluorinated compounds and long chain alkanes are common substances for constructing low surface energy surfaces. However, long chain perfluorinated compounds are highly persistent, difficult to degrade in the environment, and pose pollution hazards to human health and the environment by accumulating in the environment, drinking water, and food [23]. This requires careful consideration in its use. Compared to long-chain alkanes, perfluorinated compounds has stronger hydrophobic and oleophobic properties, and more stable performances in extremely fouling environments [24]. PFA has long-term environmental concern and its use should be carefully considered. However, considering the ultra-low surface energy and excellent hydrophobicity brought about by its modification, it is still of great interest to study the performances of PFA [25–28]. On the superhydrophobic surface of Cassie-Baxter state, an air layer is trapped in the in interface of the droplet and surface [29]. The air layer effectively prevents liquid from wetting the surface, and pollutants cannot pass through the air layer to contact the surface, thereby greatly reducing the occurrence of fouling and corrosion [30]. However, the physical barrier effect of superhydrophobicity would be gradually alleviated under external disturbances, therefore wettability control strategy alone cannot provide the antifouling activity for a relatively long term [31].

In response to the complex marine environments and physical damage threats, the strategy of combining multiple antifouling functions is of great interest [32]. Among the known antifoulants, capsaicin is a natural alkaloid widely found in chili and pepper [33]. Its unique spicy flavor can inhibit the growth and reproduction of bacteria, algae and other marine organisms at appropriate concentration [34,35]. Thus, capsaicin can be used as natural additives to enhance the antifouling properties of surface coatings [36–38]. However, limited by many variables like large-scale fabrication difficulties, capsaicin extraction raised the concerns of cost efficiency [39]. Alternatively, many researchers have successful in synthesizing capsaicin-mimicking monomers such as N-(2-hydroxyl-3-methyl acrylamide-4, 6-dimethyl benzyl) acrylamide (HMDA) [40] and N-(5-methyl acrylamide-2,3,4 hydroxy benzyl) acrylamide (AMTHBA) [41]. Zhang et al. [42] prepared an antifouling coating via grafting zwitterionic ester and capsaicin copolymers onto polydimethylsiloxane (PDMS). Under the dual functions offered by zwitterions and capsaicin, this coating can reduce the adhesion of proteins, bacteria and diatoms by 88.5 %, 99.0 % and 99.5 %, respectively. Hao et al. [43] fabricated pH-response multilayer films with capsaicin release capacity. The $(ALG/CAP@CS)_m$ films were reported to have the best long-term antibacterial performance by adjusting the release rate of capsaicin. The above studies have demonstrated the good antibacterial performance of synthesized capsaicin. The antifouling activity of the capsaicin-containing coatings is yet far from the actual marine application requirements, for the marine environment involves harsh corrosive media and thousands of fouling species. To combat the harsh marine environment, developing the antifouling coating with multiple anti-fouling/corrosion functions is essentially required [10]. In addition to the use of capsaicin as the antifoulant, constructing surface superhydrophobicity would facilitate to a large extent the desired performances of the coatings.

In this study, capsaicin-mimicking N-(4-hydroxy-3-methoxy-benzyl)-acrylamide (HMBA) was synthesized and further polymerized with silane. To build the micro-nanostructure, silica nanoparticles were added in the polymerized HMBA. A multi-layered coating system that consists of uncured epoxy as the bottom layer, fluorinated epoxy with HMBA-silica (HS) as the middle layer and fluorinated epoxy with high content HS as the top layer was constructed on 316 L substrate. Morphologies of the coatings have been characterized, and the effect of their surface roughness and surface chemical composition on wettability was investigated. Influence of the capsaicin content in the coatings on their antibacterial performances was elucidated by examining the behaviors of incubated *E. coli* and *S. aureus*. The low adhesion of proteins, polysaccharides, bacteria and algae property on the superhydrophobic coating was also evaluated by observing their immobilization on the surface. In addition, electrochemical measurements including electrochemical impedance spectroscopy (EIS) and potentiodynamic polarization (PDP) were carried out to study the anti-corrosion behaviors of 316 L substrate, the epoxy coating and the HS coatings.

2. Materials and methods

2.1. Materials

316 L steel substrate was purchased from local market and washed with acetone before use. SiO_2 (20 nm, 99.5 % purity), SiO_2 (50 nm, 99.5 % purity), α-cellulose (25 μm), guaiacol (>99.0 % purity) and N-methylolacrylamide (98 % purity) were purchased from Macklin Reagent Co., Ltd.. Tetraethyl orthosilicate (98 %), 1H,1H,2H,2H-Perfluorodecyltrimethoxysilane (FAS, 98 % purity), aluminum chloride anhydrous (98 % purity), N-[3-(trimethoxysilyl)propyl]ethylenediamine (TPEDA, 95 % purity), triethoxyvinylsilane (TEOVS, 97 % purity), 2,2′-azobis(2-methylpropionitrile) (AIBN, purity), bovine serum albumin (BSA, 96 % purity), sodium alginate (SA, AR), fluorescein isothiocyanate (FITC) and glutaraldehyde (50 % purity) were supplied by Aladdin Reagent Co., Ltd.. Absolute ethanol (AR), aqueous ammonia (AR), hydrochloric acid (AR) and trichloromethane (AR) were purchased from Sinopharm Reagent Co., Ltd.. Bisphenol-A-based epoxy resin (E51) was bought from Nanjing XingChen Synthetic Material Co., Ltd.. All the chemicals/materials/reagents were used as received.

2.2. Synthesis of HMBA

N-(4-hydroxy-3-methoxy-benzyl)-acrylamide (HMBA) was synthesized via the Friedel-Crafts reaction. In brief, 49.6 g (0.4 mol) guaiacol, 60.1 g (0.6 mol) N-methylolacrylamide and 50 mL trichloromethane were added in a 250 mL three necked flask and stirred at 35 °C until completely dissolved. 8.0 g aluminum chloride anhydrous was added in four times with an interval of 6 h. The mixture was continuously stirred for 7 days. After the reaction, the mixture was filtrated and washed with dilute hydrochloric acid and followed by water to get a white precipitate. Then the crude product was further recrystallized from ethanol to get pure powder.

2.3. Synthesis of PHS

Poly(HMBA-TEOVS) (PHS) was synthesized via a free-radical polymerization reaction. 10.4 g (0.05 mol) HMBA and 9.5 g (0.05 mol) TEOVS were dissolved in 100 mL ethanol. The mixture was stirred at 65 °C for 1 h under N_2 protection. Then 164 mg AIBN was added to the solution to initiate the reaction. After 24 h reaction, the solution was concentrated through a rotary evaporator and precipitated in deionized water to get yellow powder.

2.4. Preparation of superhydrophobic HS coating

The superhydrophobic HMBA-silane (HS) coating was prepared via a three-step spray method. For the bottom layer preparation, 2 g epoxy resin was dissolved in 10 mL ethanol and stirred for 1 h. Then 0.8 mL TPEDA as curing agent was added into the solution and reacted for 30 mins at 60 °C. For making the subsequent middle layer, 0.15 g SiO_2 (20 nm), 0.15 g SiO_2 (50 nm), 0.15 g α-cellulose and a specific amount of PHS were dispersed in 30 mL absolute ethanol and 10 mL aqueous ammonia mixed solution by ultrasonic for 10 mins and stirred for 30 mins at 60 °C. Then the specific amount of TEOS and FAS was added to the solution and stirred for 2 h. Meanwhile, 3 g epoxy resin was dissolved in 15 mL ethanol and stirred for 1 h. After that the two solutions were blended and 0.3 mL TEOS and 0.3 mL FAS were added and further stirred for 1 h. At the same time, 1.2 mL TPEDA and 0.3 mL FAS were dissolved into 10 mL ethanol as curing agent in another container and reacted for 1 h. Finally, the curing agent was added to resin solution and reacted for 15 mins to get a homogeneous solution. The specific formula is listed in Table S1. For fabrication of the top layer, 0.3 g SiO_2 (20 nm), 0.3 g SiO_2 (50 nm), 0.3 g α-cellulose and a specific amount of PHS were dispersed in 30 mL absolute ethanol and 10 mL aqueous ammonia mixed solution by ultrasonic for 10 mins and stirred for 30 mins at 60 °C. Then the specific amount of TEOS and FAS was added to the solution and stirred for 2 h. Meanwhile, 2 g epoxy resin was dissolved in 10 mL ethanol and stirred for 1 h. After that the two solutions were blended and 0.3 mL TEOS and 0.3 mL FAS were added and further stirred for 1 h. At the same time, 0.8 mL TPEDA and 0.3 mL FAS were dissolved into 10 mL ethanol as curing agent in another container and reacted for 1 h. Finally, the curing agent was added into resin solution and reacted for 15 mins to get the homogeneous solution. The specific formula is listed in Table S1.

The spray processing was carried out via a spray gun, and the spray distance was controlled at 15 cm and the spray pressure was set at 0.7 MPa. 20 mL bottom layer solution, 20 mL middle layer solution and 20 mL top layer solution were sprayed in turn onto 100 cm^2 substrate. In between each spray, the substrate was dried at 45 °C for 10 min. Finally, the sprayed substrate was dried at 120 °C for 6 h. The key reactions involved in the fabrication of the superhydrophobic antifouling coatings are shown in Fig. 1, in which the coating fabrication was also schematically depicted.

2.5. Characterization

Nuclear magnetic resonance spectroscopy (^{1}H NMR and ^{13}C NMR) spectra of the samples were acquired by the Bruker AVANCE NEO 600 (Germany) using MeOD as solvent. Fourier transform infrared spectrometer (FTIR, Thermo Fisher IS 50, USA) was used to determine the chemical composition of the coatings. Scanning electron microscope (SEM, Hitachi regulus 8230, Japan) and energy dispersive X-ray spectroscope (EDS, Bruker XFlash 6-100, Germany) were employed to characterize the morphology and surface chemistry of the samples. Surface roughness of the coatings was measured by white light interferometer (Bruker GTK-A, Germany) with 20x magnification. Wettability and surface free energy was tested by a contact angle analyzer (Kruss DSA25E, Germany). The water droplet volume was 3 μL for water contact angle measurement as well as 5 μL for water sliding angle test. To minimize the impact of high roughness of HS coatings on surface energy measurement, HS-0 and HS-3 coatings without the addition of nano SiO_2 particles and α-cellulose were used for surface energy measurement. The surface free energy was calculated through the Wu's model [44], as shown in Eqs. (1) and (2):

$$\gamma_l(1+\cos\theta) = 4\left(\frac{\gamma_l^d\gamma_s^d}{\gamma_l^d+\gamma_s^d}+\frac{\gamma_l^p\gamma_s^p}{\gamma_l^p+\gamma_s^p}\right) \quad (1)$$

$$\gamma_s = \gamma_s^d + \gamma_s^p \quad (2)$$

Where γ_l is the liquid surface tension, θ is the contact angle, γ_s is the solid surface tension, d and p represent the polar and dispersive parts of the surface tension, respectively. Water and diiodomethane were chosen as detect liquid. Five random positions were selected for the measurement of each designated sample to get reliable results. The mechanical durability of the HS coating is tested by sandpaper abrasion. The HS-3 coating sample was put face-down onto a sandpaper (1200#), then the sample was moved for 20 cm along the ruler on the sandpaper. The water contact angle was recorded at each specific distance.

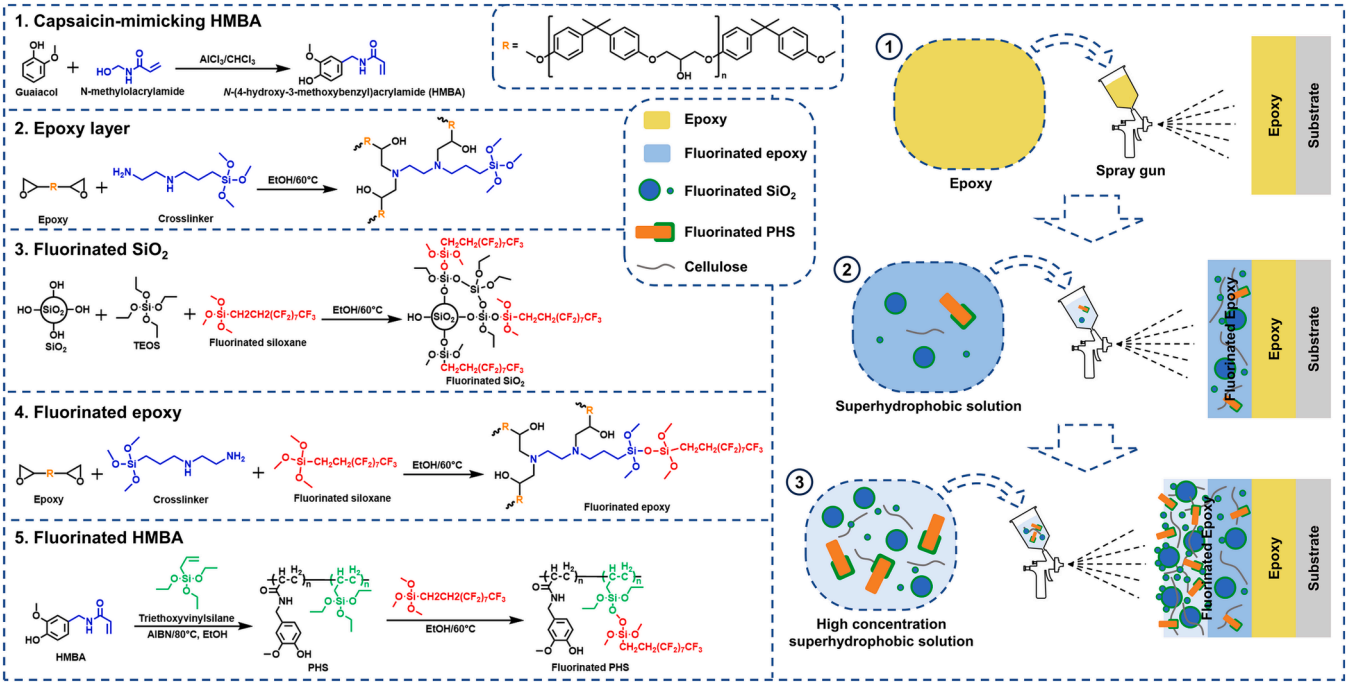

Fig. 1. The key reactions involved in fabrication of the superhydrophobic antifouling coating, and the 3-layers construction is also schematically depicted.

2.6. Protein and polysaccharide adhesion test

Bovine serum albumin (BSA) and sodium alginate (SA) were used as the typical protein and polysaccharide, respectively. BSA and SA were pre-stained with FITC. In brief, 50 mg BSA or SA was dissolved in 25 mL PBS solution at 4 °C. Then 600 μL FITC-DMSO solution (2 mg mL^{-1}) was added into the solution and reacted in the shaker at 4 °C for 3 h. After the reaction, the solution was dialyzed (M.W. 7000) at 4 °C to remove unreacted FITC. Finally, 1 mg mL^{-1} FITC stained solution was made by adding PBS solution to 50 mL. Coating samples were placed in a 24-well plate, then 1 mL BSA-FITC or SA-FITC solution was added, respectively. After incubation at 4 °C for 24 h, the coatings were rinsed with PBS solution twice and dried with nitrogen. The adhesion of BSA-FITC and SA-FITC on the coating was observed using a laser confocal microscope (LCMS, Leica TCS SP8, Germany) with the measurement wavelength ranging from 509 to 559 nm. The LCMS images were processed with ImageJ software to get the fluorescence area.

2.7. Antibacterial test

Escherichia coli (*E. coli*, ATCC25922) and *Staphylococcus aureus* (*S. aureus*, CMCC(B)26069) were used as representatives of gram-negative and gram-positive bacteria, respectively. Bacteria proliferated overnight in the culture medium (Luria–Bertani medium for *E. coli* and Tryptic Soy Broth medium for *S. aureus*). The media were then centrifuged and washed off with PBS buffer, and the concentration was adjusted to about 1×10^8 CFU mL^{-1}. All the samples (10 mm x 10 mm) were sterilized by a UV lamp for 30 mins and put in a 24-well plate. Afterwards 1 mL of 100 times PBS buffer diluted bacteria suspension (1×10^6 CFU mL^{-1}) was added to the plate. After being incubated at 37 °C for 12 h, 100 μL of bacteria suspension was diluted for another 100 times with PBS buffer and then dispersed in solid medium petri dish at 37 °C for 18 h incubation. Incubating bacteria at 37 °C is a widely used protocol for rapid growth of the bacteria, even though there are concerns about the differences between sea temperature and the relatively high incubation temperature. Some researchers realized that a decrease in temperature between from 37 °C to 20 °C affected the growth rate of bacteria, but there was little change in final yield and adhesion of the bacteria [45,46]. Our previous preliminary experiments showed similar phenomena (data not shown). The antibacterial performance was judged by counting the colonies number of the medium.

2.8. Bacteria adhesion test

The prepared samples were sterilized by a UV lamp for 30 mins and put in a 24-well plate. 1 mL concentrated bacteria suspension (1×10^8 CFU mL^{-1}) was added into each well and incubated at 37 °C for 12 h. During the incubation, 100 μL bacteria suspension was taken out every 4 h to measure the optical density (OD_{600}) value at 600 nm. After 24 h incubation, the suspension was removed, and the samples were carefully washed with 1 mL PBS buffer for two times and divided into two groups. One group of the samples was transferred into a new 24-well plate containing 1 mL PBS buffer each well and ultrasonication treatment was carried out for 5 min to remove any bacteria adhered on the surface. 100 μL ultrasonicated suspension was taken out and dispersed in solid medium petri dish at 37 °C for subsequent incubation for 18 h. The colony number was counted by plate counting method. 1 mL 2.5 vt% glutaraldehyde solution was added into another group and stored at 4 °C for 24 h to immobilize bacteria. Then glutaraldehyde solution was removed and washed twice with 1 mL deionized water. The samples were washed sequentially with 10 vt% (5 min), 25 vt% (5 min), 50 vt% (5 min), 75 vt % (5 min), 90 vt% (5 min) and pure ethanol solution (10 min, two times) to dehydrate and were further dried in a 37 °C oven for 48 h. The bacteria adhered on the surfaces of the samples were characterized by SEM.

2.9. Algae adhesion test

Chlorella was used for the algae adhesion test. The algae number in the suspension was adjusted to 1×10^6 CFU mL^{-1} in PBS solution. Coating samples were placed in a 24-well plate, then 1 mL algae solution was added in for the following incubation in a climatic incubator with a 12:12 h L/D cycle conducted at 27 °C. After 24 h, the coating samples were rinsed twice with PBS solution and were subsequently immersed in 2.5 % glutaraldehyde for 24 h to fix the adhered algae. Then 1 mL deionized water was used to wash the sample twice. The samples were then washed sequentially with 10 vt% (5 min), 25 vt% (5 min), 50 vt% (5 min), 75 vt% (5 min), 90 vt% (5 min) and pure ethanol solution (10 min, two times) to dehydrate and further dried in a 37 °C oven for 48 h. The samples were observed by LCMS with the measurement wavelength ranging from 468 nm to 508 nm. The LCMS images were processed with ImageJ software to get the fluorescence area.

2.10. Electrochemical corrosion test

Electrochemical impedance spectroscopy (EIS) and potentiodynamic polarization (PDP) curves were acquired using an electrochemical workstation (ChenHua, CHI660E, China). All the samples were immersed in artificial seawater for 12 h before the test. All the measurements were carried out after achieving steady-state open circuit potential (OCP) conditions. The EIS experiment used the frequency range of $10^{-2} \sim 10^5$ Hz and the amplitude of 10 mV. For the PDP testing, the potential range was −0.4 mV to 0.4 mV (vs. OCP), and the scan rate was 10 mV s^{-1}.

2.11. Real sea test

Real sea test was performed at a port (29.8863 N, 121.9972E, Beilun Ningbo, China) in East China Sea from July 16th, 2023 to September 14th, 2023. The Q235 substrate (100 mm x 100 mm x 4 mm) was sandblasted and further coated polybenzoxazine. Bare Q235 plate was used as the blank sample. The samples were immersed in seawater at a depth of 0.2–2 m. At every 30 days, samples were taken out of the sea for photography and re-placed back in the sea for further testing.

3. Results and discussion

Capsaicin-mimic N-(4-hydroxy-3-methoxy-benzyl)-acrylamide (HMBA) powder was successfully synthesized via the Friedel-Crafts reaction and its molecular structure was determined by proton nuclear magnetic resonance (^{1}H NMR) and carbon nuclear magnetic resonance (^{13}C NMR). As shown in Fig. 2A, the ^{1}H NMR (MeOD, 600 MHz) spectra showed the δ peaks at 3.84 ppm (s, 3H, O—CH_3, 7), 4.34 ppm (d, 2H, CH_2—NH, 9), 5.66 ppm (t, 1H, CH═, 2), 6.26 ppm (d, 2H, CH_2═, 1), and characteristic δ peaks at 6.73 ppm and 6.88 ppm (aromatic, 4, 5, 8). The δ peak at 4.34 ppm of position 9 suggests that hydroxymethyl acrylamide were successfully connected to the para-position of guaiacol. As shown in Fig. 2B, the ^{13}C NMR (MeOD, 600 MHz) curve showed the δ peaks at 44.1 ppm (—CH_2—,k), 56.3 ppm (—CH_3, h), 112.6 ppm,116.2 ppm, 121.6 ppm and 131.1 ppm (aromatic, i, e, d, j), 127.8 ppm (CH_2═, a), 132.1 ppm (CH═, b), 147.0 ppm and 149.1 ppm (═C—O, f, g), and 167.9 ppm (C═O, c). The appearance of peak k at 44.1 ppm proves the successful synthesis of HMBA.

FTIR spectra of the synthesized HMBA is shown in Fig. 2C. The peak located at 3325 cm^{-1} is attributed to the hydroxyl groups on the benzene ring stretching vibrations. The wavenumbers of 3099 cm^{-1}, 1595 cm^{-1} and 1523 cm^{-1} are assigned to the stretching vibrations of —C═C— bonds. The —CH_2— bonds peaks are located at 2965 cm^{-1} and 2836 cm^{-1}, which further suggests the successful synthesis of HMBA [39].

Topographical SEM morphologies of the epoxy, the HS-0 and the HS-3 coatings are shown in Fig. 3A and Figure S1. There are lots of shallow pits on the surface of the epoxy, presumably generated by the high-speed

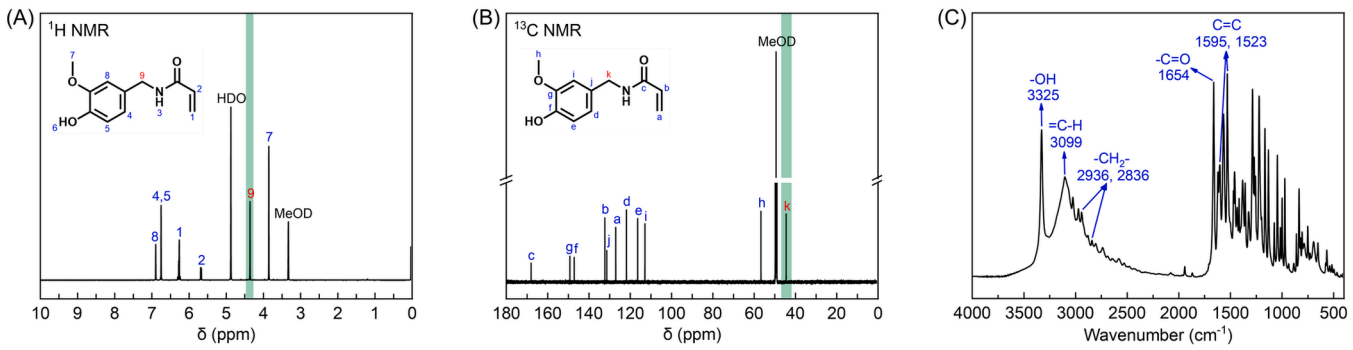

Fig. 2. ^{1}H NMR spectrum (A), ^{13}C NMR spectrum (B), and FTIR spectrum (C) of the synthesized HMBA.

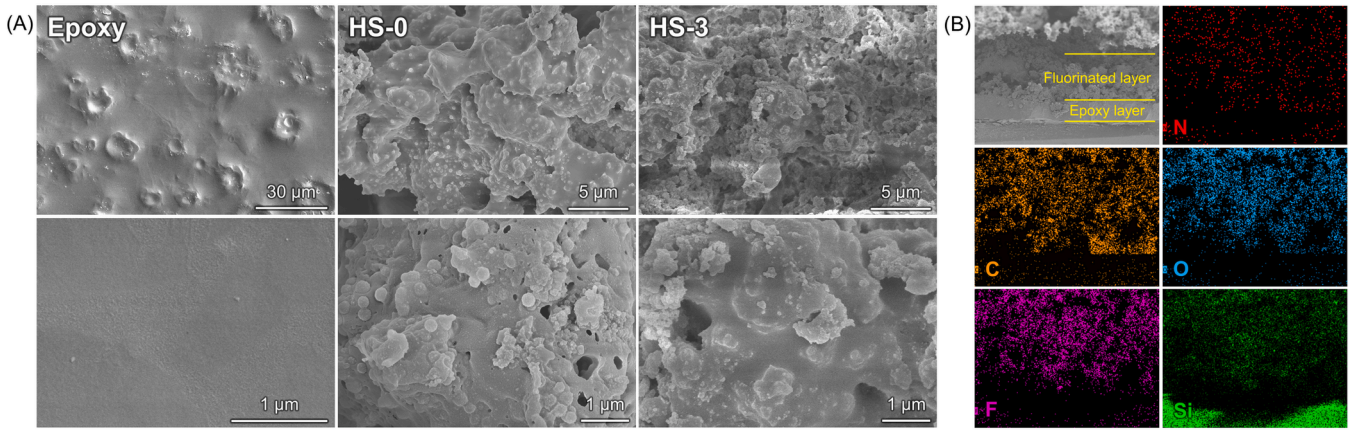

Fig. 3. (A) Topographical SEM images of the epoxy, the HS-0 and the HS-3 coatings, (B) cross-sectional SEM images and EDX images of the HS-3 coating.

impact of liquid droplets during the spray processing. On a smaller scale, the epoxy surface shows a smoother feature. For the HS series coatings, their surfaces are lotus-like and rough, also many small SiO_2 spheres protrude on the surface, resulting in a high roughness surface. For better characterization of the cross-sectional structure, the HS-3 coating was sprayed on a neat silicon chip and fractured in liquid nitrogen, the SEM and EDX images are shown in Fig. 3B. It is clear that the bottom dense layer is composed of epoxy. The edge in between the epoxy layer and the fluorinated epoxy layer is clearly seen. However, due to the similar composition of the middle layer and the top layer, their interface is ambiguous. From the EDX images, it is noted that the addition of fluorinated silane and SiO_2 increased the content of O, F and Si elements from the bottom layer all the way to the top layer. This fluorinated top surface could effectively reduce the surface free energy of the coatings.

The chemical composition and structural features of the as-prepared coatings were examined by FTIR and the spectra were shown in Figure S2. The peaks at 460 cm^{-1} and 1073 cm^{-1} are ascribed to the Si—O stretching vibrations and the Si—O—Si stretching vibrations, respectively, suggesting the presence of a great number of silica and silane in the HS-0 and the HS-3 coatings. The peak at 1204 cm^{-1} is assigned to the C—F bonds, indicating successful fluorosilane modification of the coatings. The intensity of the amide bond peak at 1650 cm^{-1} is gradually increased as comparing the HS-0 coating with the HS-3 coating, which is a result of the addition of PHS powder.

Surface roughness usually plays important role in regulating biological performances of antifouling coatings. Surface roughness of the coatings was characterized by a white light interferometer and evaluated by arithmetic mean deviation (Ra). As shown in Fig. 4, the Ra value of the bare 316 L is 0.14 μm, after the epoxy coating deposition, augmentation of the Ra value to 1.70 μm was seen. Coarse surface of the substrate usually facilitates adhesion of the coating. For the further fabricated superhydrophobic antifouling coatings, the Ra values of the HS-0 and the HS-3 coatings are greatly increased to 5.79 μm and 7.93 μm, respectively. According to the Cassie-Baxter model, roughness and surface free energy are the key factors affecting the hydrophobicity of the surface [47]. A more robust air cushion layer would be readily formed through absorbance on the non-ideal hydrophobic solid surface with a higher Ra value, this air barrier could help prevent the entrance of liquid, bacteria and other fouling microorganisms [48].

Wettability of the coatings was further examined. Water contact

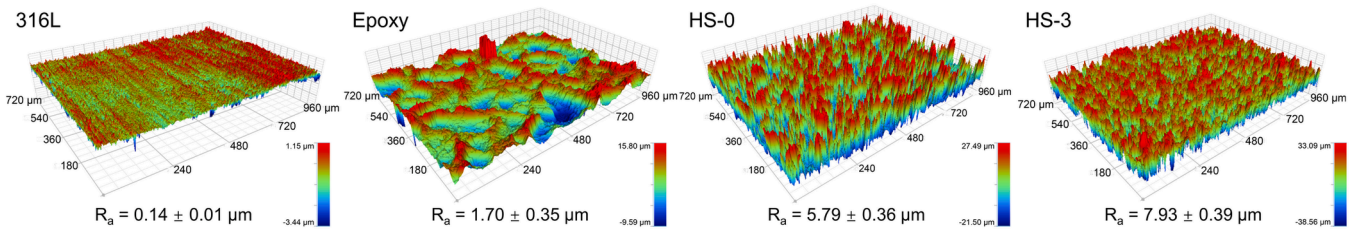

Fig. 4. Roughness images of the 316 L plate, the epoxy coating, the HS-0 coating, and the HS-3 coating.

angle (WCA) and water rolling angle were measured by a contact angle analyzer. As shown in Fig. 5A, the pristine 316 L and the epoxy coating are hydrophilic, their WCAs are below 90° and all rolling angles are higher than 10°. After deposition of the fluorinated epoxy coating, the WCAs of the HS coatings are all higher than 160° (164° for the HS-3 coating) and the sliding angles are 6.1° and 7.4° for the HS-0 coating and the HS-3 coating, respectively. The HS coating reached a superhydrophobic state. Fig. 5B shows the apparent surface free energy values of the coatings, for the testing, water and diiodomethane were used as detecting liquid, the Wu's model was chosen as the calculating model [44]. The apparent surface free energy of the 316 L substrate and the epoxy coating is 42.16 mN m^{-1} and 57.23 mN m^{-1}, respectively. However, the HS-0 coating and the HS-3 coating show a smaller surface free energy of 13.9 mN m^{-1} and 4.9 mN m^{-1}, respectively. The reason likely lies in the fact that the content of perfluorosilane in the HS-3 coating is twice that of HS-0 coating, and more carbon fluorine bonds lead to more surface energy reduction. Such a low surface free energy is not conducive to the spreading of liquids and adherence of fouling species, in turn greatly reducing the possibility of occurrence of biofouling and corrosion [49]. The mechanical durability of the HS coating was evaluated by sandpaper abrasion test. Insets of Fig. 5C show the test process of sandpaper abrasion. The HS-3 coating sample with 100 g loading was moved on a sandpaper (1200#) along the ruler direction. The change of WCA was measured after each specific distance of movement. As shown in Fig. 5C, WCA of the HS-3 remains at 160° after being abraded for 400 cm, and its WCA only got decreased by about 3° and remained higher than 155° after 1000 cm sandpaper abrasion. The mechanical durability of the superhydrophobic coatings is also compared with the data reported in other literatures (Table 1). The HS-3 coating showed relatively long-term superhydrophobicity in the sandpaper abrasion circumstances.

In addition to the physicochemical features of the coatings, their adhesive strength was also measured according to the standard ISO 2409:2020. In brief, a dedicated multi-tooth cutter (BGD 504/2) with 1 mm interval was used to scratch through the coating to create vertical grid. Then 3 M tape (Scotch 600) was stuck on the coating and compressed with a 2 kg load for 2 min, followed by being peeled off from the coating. The surface of destroyed coating was observed by SEM. As shown in Fig. 6A, the edge of the scratches is clear, and the structure of the coating keeps intact and no obvious defects are seen, meeting the highest standards in ISO 2409:2020. Interestingly, there is no difference in the coating integrity between the HS-0 coating and the HS-3 coating, indicating that the addition of HMBA did not affect the adhesive strength of the superhydrophobic coating. After scratch test, the hydrophilicity of the HS-0 and the HS-3 coatings was characterized. As shown in Fig. 6B, water droplets cannot smoothly roll off HS-0 coating, part of droplets sticked to the scratches. Meanwhile, the WCA on the scratches was decreased to about 145°. On the other hand, water droplets still rapidly rolled off HS-3 coating without leaving any traces. The WCA of HS-3 maintained about 166°.This result indicates that HS-3 has better resistance to mechanical wear compared to HS-0. During the preparation process, HS-3 used a larger amount of fluorosilane and silane coupling agents, the hydrophobic part of the coating is thicker than HS-0 coating.

Table 1
Comparison of the mechanical durability of the HS-3 superhydrophobic coating with other reported coatings.

Mechanical abrasion parameters	Wettability	Reference
Sandpaper (1200#) abrasion with 100 g weight for 1000 cm.	WCA decrease of 3°	This work
Sandpaper abrasion for 600 cycles	WCA decrease of 20.03°	[48]
Sandpaper (1000#) abrasion with 50 g weight for 200 cm.	WCA decrease of 4°	[50]
Sandpaper (800#) abrasion 1000 cycles under 45 kPa (20 cm for a cycle).	WCA maintained at 152°	[51]
Sandpaper abrasion with 100 g weight for 10 cm.	Remained superhydrophobic	[52]

In the marine environment, biofouling is usually initiated by attachment and following colonization of microorganisms like algae and bacteria, which in most cases is accelerated by the conditioning layer of adhered proteins and polysaccharides. The macromolecules conditioning layer regulates to the most extent the formation and evolvement of biofilm [1]. Therefore, inhibiting the adsorption of organic macromolecules is an efficient measure to prevent the occurrence of biofouling in the first place [53]. In this study, FITC stained bovine serum albumin (BSA) and FITC stained sodium alginate (SA) were used as representative proteins and polysaccharides, respectively. The coating samples were co-incubated with BSA-FITC and SA-FITC, respectively, then observed by laser confocal microscope. As shown in Fig. 7A, there are almost no fluorescent dots on the bare 316 L substrate due to its smooth surface and weak chemical bonding. In comparison, a large area was covered by fluorescent proteins on the epoxy coating, predominately because of the high surface free energy and high chemical activity of the epoxy coating. After being coated with the superhydrophobic epoxy, the adhesion of fluorescent protein is effectively mitigated on the HS-0 coating, and the HS-3 coating exhibits the same protein adsorption level as the 316 L substrate. For the SA-FITC, similar adsorption behavior was revealed. In addition, the inhibited adhesion of the typical macromolecules was quantitatively evaluated by calculating the covered area. As shown in Fig. 7B, the adsorbed BSA-FITC covered 16.6 % and 97.3 % of the surface of the 316 L plate and the epoxy coating, respectively, and the adsorbed SA-FITC covered 8.5 % and 95.1 % of the surface of the 316 L plate and the epoxy coating, respectively. However, it is noted that after the superhydrophobization treatment, the HS-3 coating showed dramatically reduced adhesion of BSA-FITC and SA-FITC on its surface to 11.9 % and 8.7 %, respectively. These results indicate that the HS coatings have pronounced activity of resisting adhesion of proteins and polysaccharides. HS-3 has a stronger

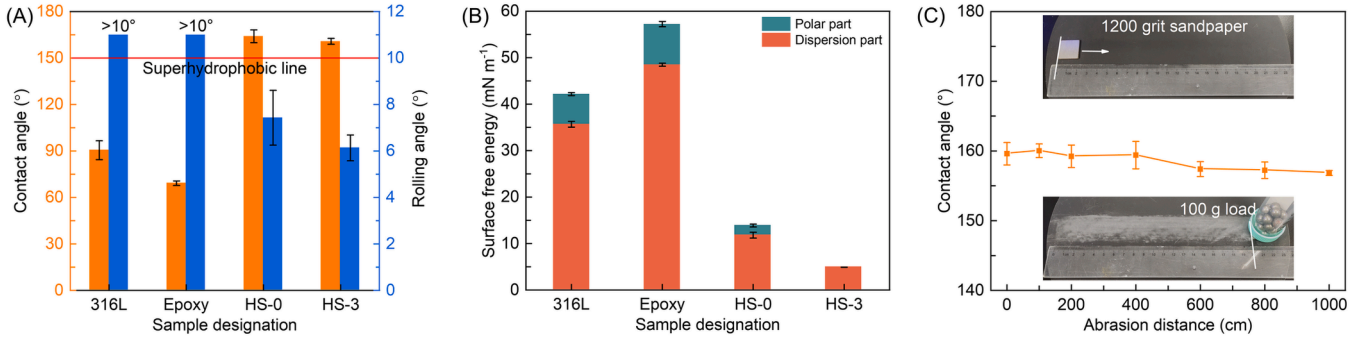

Fig. 5. (A) Water contact angle and sliding angle. (B) Surface free energy calculated through the Wu's model. (C) Sandpaper abrasion test of the HS-3 coating (inset images show the sandpaper abrading process).

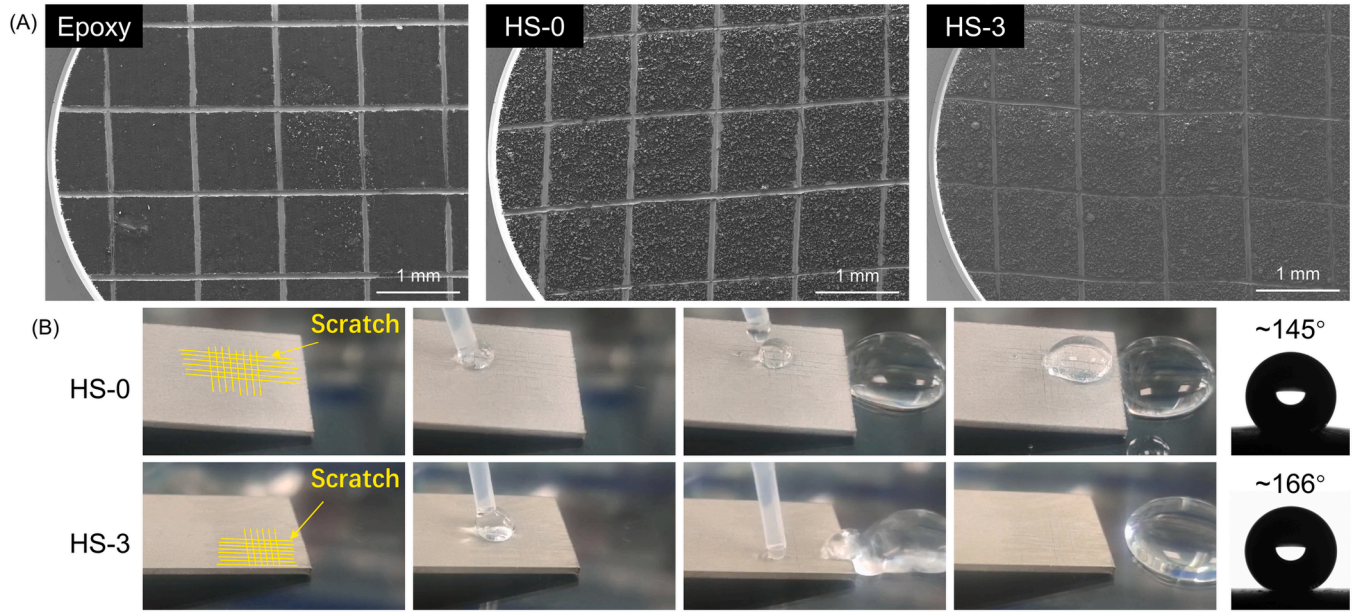

Fig. 6. (A) SEM images of the epoxy coating, the HS-0 coating and the HS-3 coating after the adhesion test. (B) Water rolling test after scratch.

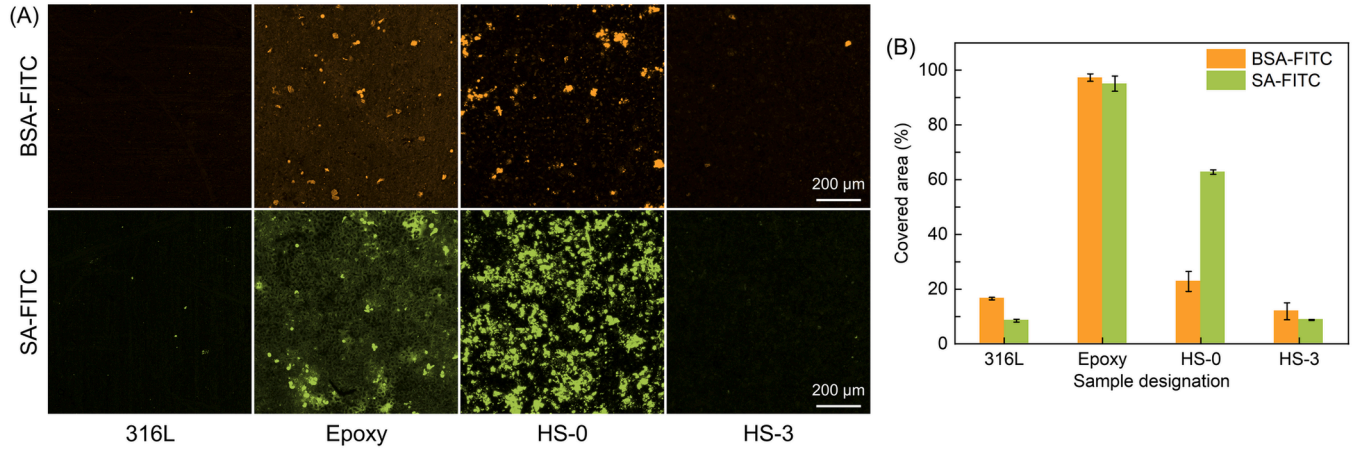

Fig. 7. (A) Laser confocal microscope images of BSA-FITC and SA-FITC adsorbed on the different coatings after 24 h incubation. (B) Statistical coating surface area covered by BSA-FITC and SA-FITC after 24 h incubation testing.

superhydrophobic structure, which is beneficial for maintaining its liquid repellency even after part of surfaces are contaminated with proteins and polysaccharides. For a hydrophobic surface, upon contacting with water, an air cushion layer is usually formed, due mainly to the fact that water drop cannot penetrate into the small cavities between micro-nanostructure [54]. This solid−air−liquid heterogeneous interface could physically isolate the contact of water with the surface, thereby delaying the adhesion of macromolecules and the formation of

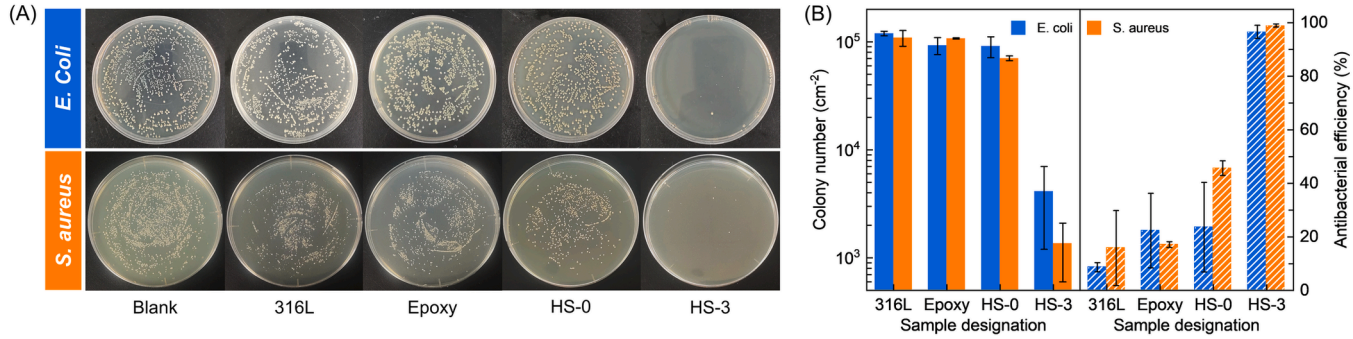

Fig. 8. (A) Digital photos of *E. coli* and *S. aureus* incubated with the different coatings for 12 h, and (B) statistical colony number and antibacterial efficiency measured using the plate counting method.

conditioning layer [54]. While the conditioning layer in most cases facilitates the formation of biofilm, accelerating the evolvement of biofouling.

To assess the antifouling activity of the coatings, their antibacterial performances were typically investigated. For the testing, the coatings were co-incubated with the suspension of the gram-negative bacteria *E. coli* and the gram-positive bacteria *S. aureus*. As shown in Fig. 8A, the 316 L substrate, the epoxy and the HS-0 coatings triggered formation of large number of *E. coli* colonies. In comparison, however, only few colonies could be observed for the HS-3 coating. For the bacteria *S. aureus*, the same trend was observed, that is, many colonies propagate on the epoxy coating and the HS-0 coating, and bacteria struggle to survive on the HS-3 coating. As shown in Fig. 8B, the colony number of *E. coli* for the 316 L substrate, the epoxy coating and the HS-0 coating is all approximately in the order of 10^5, and the antibacterial efficiency against *E. coli* of the 316 L substrate, the epoxy coating and the HS-0 coating is 8.7 %, 22.4 % and 23.6 %, respectively. The situation with *S. aureus* is also similar. Strikingly, the HS-3 coating showed the capability of killing 96.6 % *E. coli* and 99.0 % *S. aureus*, meanwhile, the number of bacterial colonies decreased by three orders of magnitude, suggesting the exciting synergistic antibacterial performances of the superhydrophobicity of and the synthesized antifoulant in the HMBA coating.

Antibacterial performances of the HS coating with different HMBA content were further investigated and the result is listed in Figure S3. The HS-0.5 coating, the HS-1 coating, and the HS-2 coating showed the sterilizing efficiency against *E. coli* of 66.8 %, 42.8 % and 33.3 %, respectively. Inspiringly, when the PHS content in the coatings was augmented (i.e. for the HS-3 coating), the antibacterial efficiency dramatically increased to 96.6 %, indicating that at low concentrations, the addition of the synthesized capsaicin would benefit the growth of adhered bacteria, and after certain threshold level, high concentrations of the capsaicin (10 wt.% PHS in top layer) would effectively inhibit the proliferation of the Gram negative bacteria. For the *S. aureus* bacteria, however, the HS coatings showed an increased antibacterial rate with augmented capsaicin content, the HS-3 exhibits an antibacterial efficiency of 99.0 %. It was believed that *S. aureus* lacks outermost membrane that comprises lipopolysaccharides for additional protection [55]. The amide and phenolic hydroxyl groups in HMBA could change the permeability and induce rupture of the cell membrane, in turn exposing the substance of bacteria cells and inhibiting the growth and proliferation of bacterial cells [55,56]. Our experiment confirms the desired antibacterial performance of the HMBA-containing coating.

To further determine whether the bacteria were killed by the antimicrobial HMBA, the samples were incubated in a highly concentrated bacteria suspension, the optical density (OD_{600}) value at 600 nm of the suspensions was monitored, then the samples were carefully washed and ultrasound-treated to remove any adhered bacteria. The sonicated solutions were further incubated and bacteria number was counted using the plate counting method. The changes of OD_{600} values are shown in Fig. 9A. The 316 L substrate and the epoxy coating have the same declined trend in OD_{600} values. On the other hand, the HS-0 coating and the HS-3 coating showed a faster descent speed, indicating that *E. coli* bacteria survived well on the superhydrophobic surface. As shown in Fig. 9B, all the samples exhibited a large number of *E. coli* colonies. SEM characterization clearly showed the adhesion of *E. coli* on the 316 L plate, the epoxy coating, and the HS-0 coating, but no bacteria were found on the surface of the HS-3 coating, likely due to the pronounced antibacterial performance of HMBA. For the gram-positive *S. aureus*, the lowest OD_{600} value was obtained for the HS-0 coating as compared to the 316 L substrate and the epoxy coating (Fig. 9C). With the help of HMBA, the HS-3 coating shows the lowest OD_{600} value among all the samples, only 0.0145 after 24 h incubation. As shown in Fig. 9D, there are a large number of bacteria grown on the 316 L plate as well as on the epoxy coating. When the surface becomes superhydrophobic, the bacteria do not tend to adhere. As HMBA content increases, the adhesion of *S. aureus* on the HS-3 coating further decreases. These results suggest that the superhydrophobic structure can effectively prevent the adhesion of the bacteria, even if the bacteria break through the barrier, the capsaicin-like antifoulant HMBA could kill the residual bacteria to delay

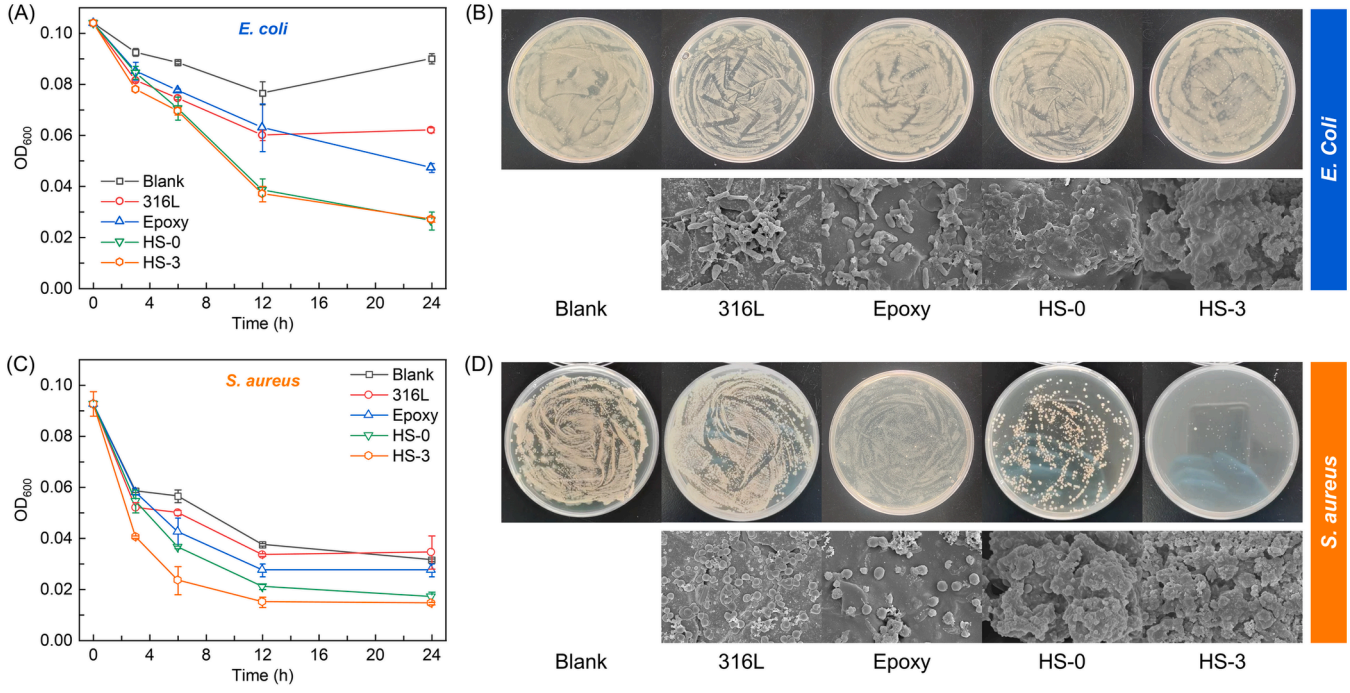

Fig. 9. (A) OD_{600} value changes of *E. coli* suspension during incubation with the samples. (B) Photographs of the colonized *E. coli* after 24 h incubation with the samples and topographical SEM images of the samples after the incubation. (C) OD_{600} value changes of *S. aureus* suspension during incubation with the samples. (D) Photographs of the colonized *S. aureus* after 24 h incubation with the samples after and SEM images of the samples after the incubation showing their topographical features.

the formation of biofilms.

During the formation of biofilms on marine structures, algae are another major fouling species besides marine bacteria. In this work *Chlorella* with the ability to survive in both seawater and freshwater was typically selected to evaluate the anti-algae performance of the coatings. As shown in Fig. 10A and B, after 24 h incubation, about 40 % area of the 316 L plate was covered by *Chlorella* and 72.7 % for the epoxy coating. The difference in adhesion ratio is presumably caused by the differences in surface topography and surface free energy. As shown in Fig. 4, the epoxy coating has a higher Ra than the 316 L substrate, which means the differences in effective surface area. On the other hand, the amount of adhered *chlorella* is positively correlated with the decrease of the contact angle and the increase of the surface free energy of the coating surface [57,58]. As shown in Fig. 5B, the epoxy coating is more hydrophilic than the 316 L substrate and has a higher surface free energy due to the hydroxyl bonds and ether bonds contained in epoxy groups. Therefore, the anchoring of *chlorella* on the epoxy coating is likely significantly enhanced. In comparison, *Chlorella* adhesion on the HS-0 coating and the HS-3 coating is significantly constrained, showing only 1.1 % and 3.3 %, respectively, indicating the excellent anti-algae performance of the HS coatings.

As depicted in Fig. 11A, the good antifouling property of the HS-3 coating is likely attributed to multiple reasons. The air cushion layer is usually trapped in the micro-nanostructure on the superhydrophobic surface, and the solid-liquid interface transforms into solid-air-liquid heterogeneous interface, resulting in the reduction of contact area and the direct contact between microorganisms and the coating surface [59]. In addition, the extremely low surface free energy of the HS coatings could easily result in chemical inertness of their surfaces. The bonding of macromolecules (i.e. proteins and polysaccharides) with the chemical groups on the coatings surfaces is significantly sluggish and fragile, thus the formation of conditioning layer and the accumulation of microorganisms (bacteria and algae in our case) can be greatly delayed. The superhydrophobic surface is also able to effectively repel physical contact and chemical adherence of the fouling microorganisms to the interface. Apart from the superphydrophobic features of the surfaces of the coatings, the capsaicin-mimicking HMBA was used as natural antifouling additives in the coatings. As shown in Fig. 11B, the amide and phenolic hydroxyl groups in HMBA change the permeability and induce disruption of bacteria cell membrane, in turn proteins and other materials within bacteria cell are constantly exposed, consequently the growth and proliferation of bacteria is inhibited [55].

For potential applications in the marine environment, corrosion resistance of the coatings is an important concern. The anti-corrosion performance of the coatings samples was evaluated through electrochemical testing in artificial seawater. Fig. 12A shows the EIS plots and fitting curves of the bare 316 L substrate and the coatings samples. The HS-0 coating and the HS-3 coating showed significantly larger diameter of capacitive arc than the bare 316 L substrate and the epoxy coating. As shown in Fig. 12B, the |Z| values at 10^{-2} Hz of the HS-3 coating and the HS-0 coating are 1.5×10^6 Ω cm^2 and 3.6×10^6 Ω cm^2, respectively, which are higher than 2 order of magnitude of that of the bare 316 L substrate. This suggests that the HS coating can provide excellent protection for bare metal substrate. In the Bode-phase angle versus frequency plots (Fig. 12C), the 316 L substrate shows only one capacitive arc within the testing frequency range. But for the epoxy coating, the HS-0 coating and the HS-3 coating, there are two time constants included in the system. The equivalent electrical circuits used to analyze the EIS results are shown in Fig. 12E, where R_s is the solution resistance, R_c and R_{ct} is the coating resistance and charge-transfer resistance, respectively. Q_{dl} and Q_c is the constant phase elements modeling the capacitance of double-layer and the coating, respectively. Since 316 L substrate is in direct contact with the solution, the R(QR) model was used to fit the data. For the coating samples, the coating layer usually effectively prevents the substrate from participating in the electrochemical reaction. Thus, using the paralleled R(Q(R(QR))) model for the coating samples is reasonable. The electrochemical fitting results are shown in Table S2. Q_{dl} value and R_{ct} value of the bare 316 L substrate are 3.28×10^{-4} F cm^{-2} and 7.54×10^4 Ω cm^2, respectively. The HS-3 coating has a lower Q_{dl} value (8.22×10^{-8} F cm^{-2}) and a higher R_{ct} value (5.62×10^{13} Ω cm^2) than the 316 L substrate, indicating the strong corrosion resistance of the HS-3 coating with the top superhydrophobic layer. Fig. 12d shows the potentiodynamic polarization (PDP) curves of the samples tested in artificial seawater. The corrosion potential E_{corr} of the 316 L substrate, the epoxy coating, the HS-0 coating and the HS-3 coating is −0.2181 V, −0.3038 V, −0.0521 V and −0.1016 V, respectively. The HS coatings show a significant positive shift of the corrosion potential E_{corr} as compared to the 316 L substrate. In addition, the corrosion current density I_{corr} of the 316 L substrate, the epoxy coating, the HS-0 coating and the HS-3 coating is 2.0×10^{-4} A cm^{-2}, 3.6×10^{-7} A cm^{-2}, 1.8×10^{-8} A cm^{-2} and 7.9×10^{-9} A cm^{-2}, respectively. The I_{corr} of the HS-3 coating decreases more than 4 order of magnitude than the 316 L substrate. The corrosion inhibition efficiency (η,%) of the HS-3 coating was estimated using the following equation,

$$\eta = \left(1 - I_{coating} \,/\, I_{bare\ 316L}\right) \times 100\% \quad (3)$$

where $I_{coating}$ and I_{bare} 316 L is the corrosion current density of the coating and the bare 316 L substrate, respectively. The inhibition efficiency (η) of the HS-3 coating was calculated to be 99.996 %. This result demonstrates the excellent anti-corrosion performance of the HS-3 coating, which is likely attributed to the insulation effect offered by the air layer trapped in the micro-nanostructure of the superhydrophobic surface.

The antifouling and anticorrosion performances of the coatings were further preliminarily evaluated in the real sea environment. The testing site is located in a port in Beilun, Ningbo, China. Fig. 13 shows the Q235 substrate coated by commercial fluorocarbon paint, the HS-0 and the HS-3 coatings before and after the immersion in the seawater for 60 days. The bare Q235 plate was completely corroded, with thick rust

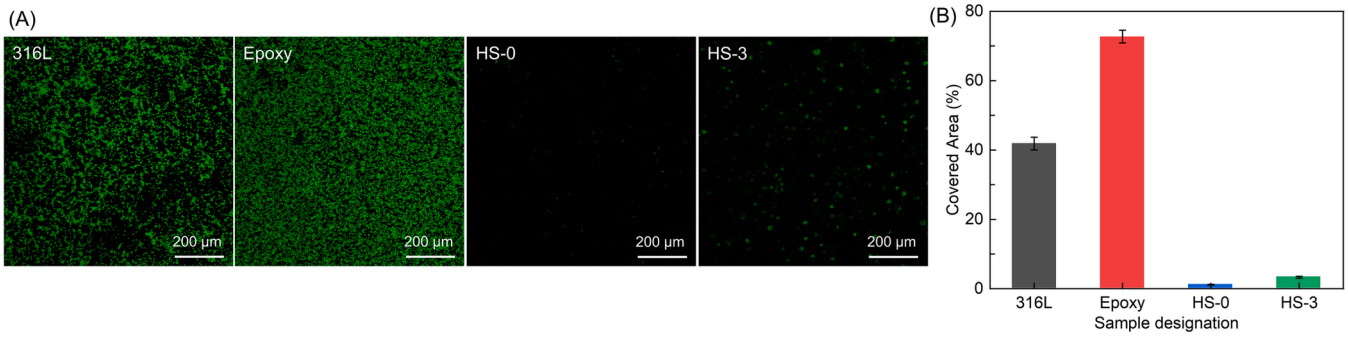

Fig. 10. (A) Laser confocal microscope images of the adhered *Chlorella* after 24 h incubation with the coatings. (B) Statistical covered area of *Chlorella* on the coatings after 24 h incubation.

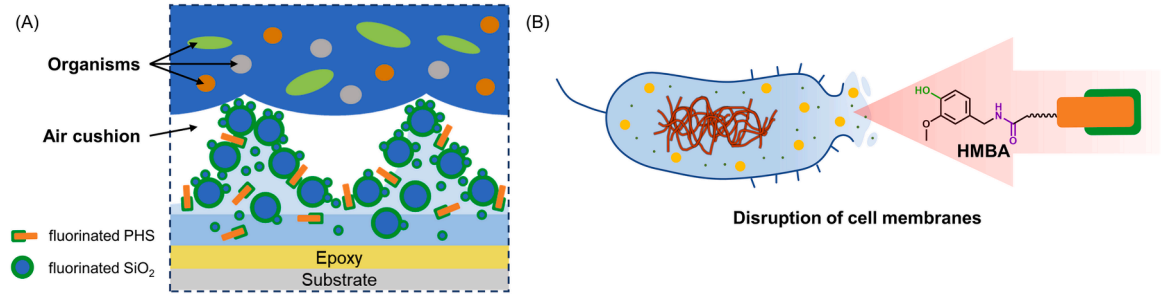

Fig. 11. (A) Schematic illustration showing water repellency and antifouling mechanism of the superhydrophobic coatings. (B) Schematic illustration showing the antibacterial mechanism of capsaicin-mimicking HMBA.

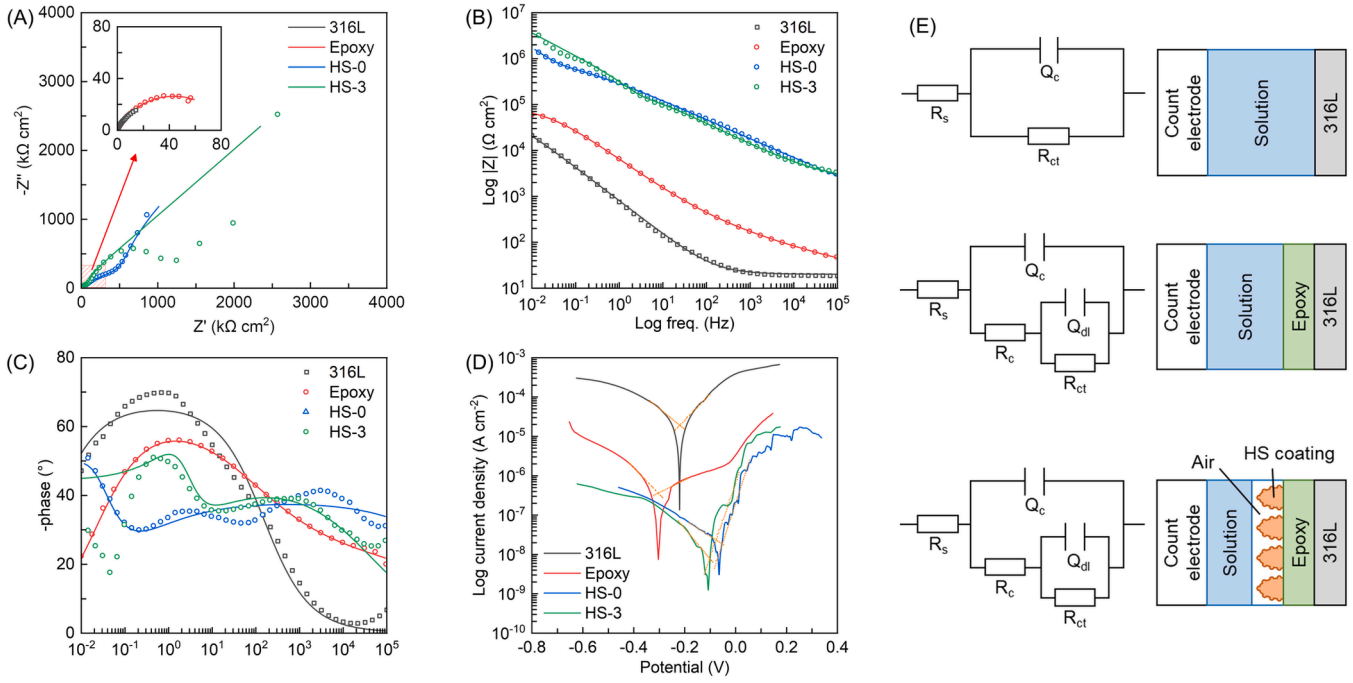

Fig. 12. (A) Nyquist plots, (d) Bode-|Z| vs frequency plots, (C) Bode-phase angel vs frequency plots and (D) potentiodynamic polarization curves of the coating samples tested in ASW solution. (E) Equivalent electrical circuits elucidating the corrosion mechanisms of the samples.

being seen on its surface at 30 days and more sludge covers the surface after 60 days. Obviously, no corrosion dot is observed on the commercial fluorocarbon paint, however, many sludges and slime were attached on the surface. The HS-0 coating got less fouling than the commercial fluorocarbon paint, but there are still some small fouling dots appeared on the surface. Inspiringly, the HS-3 coating shows very few fouling even after 60 days accumulation. These preliminary results nevertheless further suggest the excellent anticorrosion and antifouling performances of the HS-3 coating in real sea environment.

4. Conclusions

Capsaicin-mimicking N-(4-hydroxy-3-methoxy-benzyl) acrylamide (HMBA) was synthesized and used as the organic green antifoulant. The epoxy-based multilayer HMBA-silica coatings with superhydrophobic and antibiofouling functions were fabricated via a facile spray process. The rough surface structure and fluorinated epoxy of the coatings gave rise to a high water contact angle of 164° and a low sliding angle of 6°, its surface free energy was even lower than 1 mN m^{-1}. The coating with high capsaicin content exhibited outstanding capability of resisting the adhesion of proteins and polysaccharides. Significantly inhibited adherence and colonization of *E. coli* and *S. aureus* was also achieved by the capsaicin-containing superhydrophobic coating. Moreover, the newly constructed coating effectively resisted the immobilization of the algae *Chlorella*. Due to the superhydrophobicity, most of the direct contact of the fouling species with the coating was prevented, and further extinguishing phenomena were seen for the algae by the antifoulant HMBA. The inspiring antifouling performances together with the excellent anti-corrosion resistance of the capsaicin-containing superhydrophobic coating would give insight into developing environmentally friendly antifouling coatings for widespread marine applications.

CRediT authorship contribution statement

Hao Yang: Conceptualization, Methodology, Investigation, Data curation, Writing – original draft, Writing – review & editing. **Yi Liu:** Conceptualization, Writing – review & editing. **Hidetoshi Saitoh:** Writing – review & editing. **Hao Chen:** Writing – review & editing, Supervision. **Hua Li:** Conceptualization, Resources, Writing – review & editing, Supervision.

Declaration of Competing Interest

The authors declare that they have no known competing financial

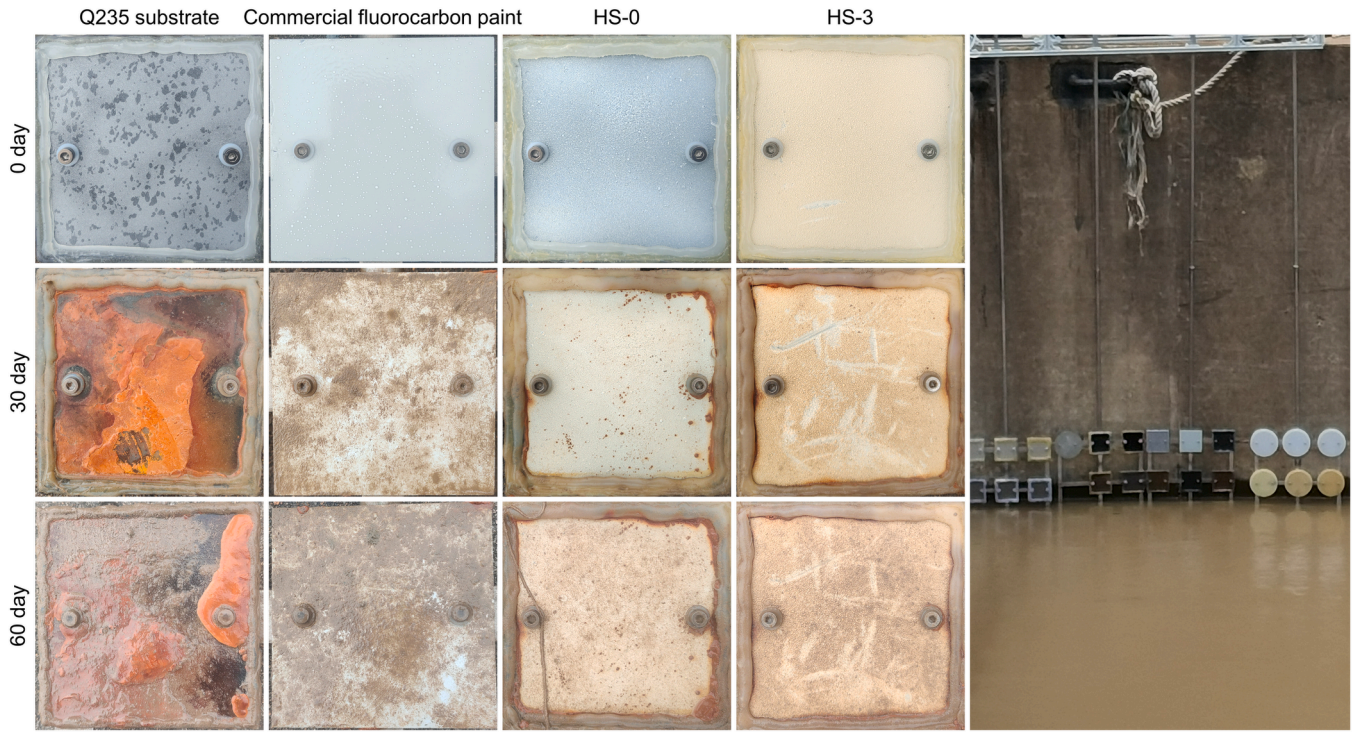

Fig. 13. Digital photos of the samples after real sea test (before the test and after 30 days and 60 days test).

interests or personal relationships that could have appeared to influence the work reported in this paper.

Data availability

Data will be made available on request.

Acknowledgments

This research was supported by the National Natural Science Foundation of China (Grant #52071329, Grant #51901107), the Key Research and Development Program of Ningbo, China (Grant #2023Z195), the Youth Innovation Promotion Association of the Chinese Academy of Sciences, China (Grant #2020299), Zhejiang Natural Science Foundation, China (Grant #LY22E010004), and S&T Innovation 2025 Major Special Program of Ningbo (Grant #2020Z095).

Supplementary materials

Supplementary material associated with this article can be found, in the online version, at doi:10.1016/j.surfin.2023.103743.

References

[1] H. Jin, L. Tian, W. Bing, J. Zhao, L. Ren, Bioinspired marine antifouling coatings: status, prospects, and future, Prog. Mater Sci. 124 (2022), 100889, https://doi.org/10.1016/j.pmatsci.2021.100889.

[2] A. Kumar, A. Al-Jumaili, O. Bazaka, E.P. Ivanova, I. Levchenko, K. Bazaka, M. V. Jacob, Functional nanomaterials, synergisms, and biomimicry for environmentally benign marine antifouling technology, Mater. Horiz. 8 (2021) 3201–3238, https://doi.org/10.1039/D1MH01103K.

[3] A.B. Asha, Y. Chen, R. Narain, Bioinspired dopamine and zwitterionic polymers for non-fouling surface engineering, Chem. Soc. Rev. 50 (2021) 11668–11683, https://doi.org/10.1039/D1CS00658D.

[4] R. Deng, T. Shen, H. Chen, J. Lu, H.-C. Yang, W. Li, Slippery liquid-infused porous surfaces (SLIPSs): a perfect solution to both marine fouling and corrosion? J. Mater. Chem. A 8 (2020) 7536–7547, https://doi.org/10.1039/D0TA02000A.

[5] L. Tian, Y. Yin, H. Jin, W. Bing, E. Jin, J. Zhao, L. Ren, Novel marine antifouling coatings inspired by corals, Mater. Today Chem. 17 (2020), 100294, https://doi.org/10.1016/j.mtchem.2020.100294.

[6] S. Susarla, G. Chilkoor, J.R. Kalimuthu, M.A.S.R. Saadi, Y. Cui, T. Arif, T. Tsafack, A.B. Puthirath, P. Sigdel, B. Jasthi, P.M. Sudeep, L. Hu, A. Hassan, S. Castro-Pardo, M. Barnes, S. Roy, R. Verduzco, M.G. Kibria, T. Filleter, H. Lin, S.D. Solares, N. Koratkar, V. Gadhamshetty, M.M. Rahman, P.M. Ajayan, Corrosion resistance of sulfur–selenium alloy coatings, Adv. Mater. 33 (2021), 2104467, https://doi.org/10.1002/adma.202104467.

[7] Y. Lin, H. Zhang, Y. Zou, K. Lu, L. Li, Y. Wu, J. Cheng, Y. Zhang, H. Chen, Q. Yu, Superhydrophobic photothermal coatings based on candle soot for prevention of biofilm formation, J. Mater. Sci. Technol. 132 (2023) 18–26, https://doi.org/10.1016/j.jmst.2022.06.005.

[8] M. Lejars, A. Margaillan, C. Bressy, Fouling release coatings: a nontoxic alternative to biocidal antifouling coatings, Chem. Rev. 112 (2012) 4347–4390, https://doi.org/10.1021/cr200350v.

[9] J. Gomez-Banderas, Marine natural products: a promising source of environmentally friendly antifouling agents for the maritime industries, Front. Mar. Sci. 9 (2022), https://doi.org/10.3389/fmars.2022.858757.

[10] X. Han, J. Wu, X. Zhang, J. Shi, J. Wei, Y. Yang, B. Wu, Y. Feng, The progress on antifouling organic coating: from biocide to biomimetic surface, J. Mater. Sci. Technol. 61 (2021) 46–62, https://doi.org/10.1016/j.jmst.2020.07.002.

[11] Y. Zuo, L. Zheng, C. Zhao, H. Liu, Micro-/Nanostructured interface for liquid manipulation and its applications, Small 16 (2020), 1903849, https://doi.org/10.1002/smll.201903849.

[12] M.S. Selim, S.A. El-Safty, M.A. Shenashen, S.A. Higazy, A. Elmarakbi, Progress in biomimetic leverages for marine antifouling using nanocomposite coatings, J. Mater. Chem. B 8 (2020) 3701–3732, https://doi.org/10.1039/C9TB02119A.

[13] P. Zhang, L. Lin, D. Zang, X. Guo, M. Liu, Designing bioinspired anti-biofouling surfaces based on a superwettability strategy, Small 13 (2017), 1503334, https://doi.org/10.1002/smll.201503334.

[14] S. Zarghami, T. Mohammadi, M. Sadrzadeh, B. Van der Bruggen, Superhydrophilic and underwater superoleophobic membranes - a review of synthesis methods, Prog. Polym. Sci. 98 (2019), 101166, https://doi.org/10.1016/j.progpolymsci.2019.101166.

[15] W. Niu, G.Y. Chen, H. Xu, X. Liu, J. Sun, Highly transparent and self-healable solar thermal anti-/deicing surfaces: when ultrathin MXene multilayers marry a solid slippery self-cleaning coating, Adv. Mater. 34 (2022), 2108232, https://doi.org/10.1002/adma.202108232.

[16] J. Yoon, M. Ryu, H. Kim, G.-N. Ahn, S.-J. Yim, D.-P. Kim, H. Lee, Wet-style superhydrophobic antifogging coatings for optical sensors, Adv. Mater. 32 (2020), 2002710, https://doi.org/10.1002/adma.202002710.

[17] J.A. Kharraz, A.K. An, Patterned superhydrophobic polyvinylidene fluoride (PVDF) membranes for membrane distillation: enhanced flux with improved fouling and wetting resistance, J. Membr. Sci. 595 (2020), https://doi.org/10.1016/j.memsci.2019.117596.

[18] B. Zhang, J. Li, X. Zhao, X. Hu, L. Yang, N. Wang, Y. Li, B. Hou, Biomimetic one step fabrication of manganese stearate superhydrophobic surface as an efficient

barrier against marine corrosion and Chlorella vulgaris-induced biofouling, Chem. Eng. J. 306 (2016) 441–451, https://doi.org/10.1016/j.cej.2016.07.062.
[19] T. Chen, Z. Wu, X. Hu, J.T. Aladejana, M. Niu, Z. Liu, Q. Wei, X. Peng, Y. Xie, B. Wu, Constructing hydrophobic interfaces in aluminophosphate adhesives with reduced graphene oxide to improve the performance of wood-based boards, Compos. Part B Eng. 198 (2020), 108168, https://doi.org/10.1016/j.compositesb.2020.108168.
[20] Z. Wang, X. Yang, Z. Cheng, Y. Liu, L. Shao, L. Jiang, Simply realizing "water diode" Janus membranes for multifunctional smart applications, Mater. Horiz. 4 (2017) 701–708, https://doi.org/10.1039/C7MH00216E.
[21] H. Zhang, X. Bu, W. Li, M. Cui, X. Ji, F. Tao, L. Gai, H. Jiang, L. Liu, Z. Wang, A skin-inspired design integrating mechano–chemical–thermal robustness into superhydrophobic coatings, Adv. Mater. 34 (2022), 2203792, https://doi.org/10.1002/adma.202203792.
[22] C.-B. Li, F. Wang, R.-Y. Sun, W.-C. Nie, F. Song, Y.-Z. Wang, A multifunctional coating towards superhydrophobicity, flame retardancy and antibacterial performances, Chem. Eng. J. 450 (2022), 138031, https://doi.org/10.1016/j.cej.2022.138031.
[23] M.G. Evich, M.J.B. Davis, J.P. McCord, B. Acrey, J.A. Awkerman, D.R.U. Knappe, A.B. Lindstrom, T.F. Speth, C. Tebes-Stevens, M.J. Strynar, Z. Wang, E.J. Weber, W. M. Henderson, J.W. Washington, Per- and polyfluoroalkyl substances in the environment, Science 375 (2022) eabg9065, https://doi.org/10.1126/science.abg9065.
[24] A.B. Tesler, S. Kolle, L.H. Prado, I. Thievessen, D. Böhringer, M. Backholm, B. Karunakaran, H.A. Nurmi, M. Latikka, L. Fischer, S. Stafslien, Z.M. Cenev, J.V. I. Timonen, M. Bruns, A. Mazare, U. Lohbauer, S. Virtanen, B. Fabry, P. Schmuki, R. H.A. Ras, J. Aizenberg, W.H. Goldmann, Long-term stability of aerophilic metallic surfaces underwater, Nat. Mater. (2023), https://doi.org/10.1038/s41563-023-01670-6.
[25] J. Shao, K. Fu, Y. Liu, S. Xu, Z. Sun, M. Cao, Y. Liu, X. Wang, Y. Zhou, Fluorine-functionalized mesoporous alumina materials with superhydrophobic surfaces, Surf. Interfaces 40 (2023), 103046, https://doi.org/10.1016/j.surfin.2023.103046.
[26] E. Korczeniewski, P. Bryk, G.S. Szymański, P. Kowalczyk, M. Zięba, W. Zięba, M. Łępicka, K.J. Kurzydłowski, S. Boncel, S. Al-Gharabli, M. Świdziński, D. J. Smoliński, K. Kaneko, J. Kujawa, A.P. Terzyk, Open sensu shaped graphene oxide and modern carbon nanomaterials in translucent hydrophobic and omniphobic surfaces – insight into wetting mechanisms, Chem. Eng. J. 462 (2023), 142237, https://doi.org/10.1016/j.cej.2023.142237.
[27] H. Zhai, X. Li, Y. Liu, J. Ji, Y. Tian, B. Wang, Y. Wei, N. Liu, L. Feng, Di-particles-derived slippery lubricant-infused porous surface with broad anti-adhesion performance, Appl. Surf. Sci. 616 (2023), 156462, https://doi.org/10.1016/j.apsusc.2023.156462.
[28] W. Li, C.-w. Chan, Z. Li, S.-Y. Siu, S. Chen, H. Sun, Z. Liu, Y. Wang, C. Hu, N. M. Pugno, R.N. Zare, H. Wu, K. Ren, All-perfluoropolymer, nonlinear stability-assisted monolithic surface combines topology-specific superwettability with ultradurability, Innovation 4 (2023), 100389, https://doi.org/10.1016/j.xinn.2023.100389.
[29] H. Jin, J. Wang, L. Tian, M. Gao, J. Zhao, L. Ren, Recent advances in emerging integrated antifouling and anticorrosion coatings, Mater. Des. 213 (2022), 110307, https://doi.org/10.1016/j.matdes.2021.110307.
[30] M.S. Selim, N.A. Fatthallah, M.A. Shenashen, S.A. Higazy, H.R. Madian, M. M. Selim, S.A. El-Safty, Bioinspired graphene oxide–magnetite nanocomposite coatings as protective superhydrophobic antifouling surfaces, Langmuir 39 (2023) 2333–2346, https://doi.org/10.1021/acs.langmuir.2c03061.
[31] G.B. Hwang, K. Page, A. Patir, S.P. Nair, E. Allan, I.P. Parkin, The anti-biofouling properties of superhydrophobic surfaces are short-lived, ACS Nano 12 (2018) 6050–6058, https://doi.org/10.1021/acsnano.8b02293.
[32] A.M.C. Maan, A.H. Hofman, W.M. de Vos, M. Kamperman, Recent developments and practical feasibility of polymer-based antifouling coatings, Adv. Funct. Mater. 30 (2020), 2000936, https://doi.org/10.1002/adfm.202000936.
[33] J.M. Janusz, B.L. Buckwalter, P.A. Young, T.R. LaHann, R.W. Farmer, G.B. Kasting, M.E. Loomans, G.A. Kerckaert, C.S. Maddin, Vanilloids. 1. Analogs of capsaicin with antinociceptive and antiinflammatory activity, J. Med. Chem. 36 (1993) 2595–2604, https://doi.org/10.1021/jm00070a002.
[34] N.P. Kalia, P. Mahajan, R. Mehra, A. Nargotra, J.P. Sharma, S. Koul, I.A. Khan, Capsaicin, a novel inhibitor of the NorA efflux pump, reduces the intracellular invasion of Staphylococcus aureus, J. Antimicrob. Chemother. 67 (2012) 2401–2408, https://doi.org/10.1093/jac/dks232.
[35] M.L.C. Rivera, N.M.A. Hassimotto, V. Bueris, M.P. Sircili, F.A. de Almeida, U. M. Pinto, Effect of Capsicum frutescens extract, capsaicin, and luteolin on quorum sensing regulated phenotypes, J. Food Sci. 84 (2019) 1477–1486, https://doi.org/10.1111/1750-3841.14648.
[36] Z. Lu, Z. Chen, Y. Guo, Y. Ju, Y. Liu, R. Feng, C. Xiong, C.K. Ober, L. Dong, Flexible hydrophobic antifouling coating with oriented nanotopography and nonleaking capsaicin, ACS Appl. Mater. Interfaces 10 (2018) 9718–9726, https://doi.org/10.1021/acsami.7b19436.
[37] J. Zhou, X. Zhang, Y. Yan, J. Hu, H. Wang, Y. Cai, J. Qu, Preparation and characterization of a novel antibacterial acrylate polymer composite modified with capsaicin, Chin. J. Chem. Eng. 27 (2019) 3043–3052, https://doi.org/10.1016/j.cjche.2019.03.024.
[38] H. Wang, J. Jasensky, N.W. Ulrich, J. Cheng, H. Huang, Z. Chen, C. He, Capsaicin-inspired thiol–ene terpolymer networks designed for antibiofouling coatings, Langmuir 33 (2017) 13689–13698, https://doi.org/10.1021/acs.langmuir.7b03098.
[39] M.D. Reyes-Escogido, E.G. Gonzalez-Mondragon, E. Vazquez-Tzompantzi, Chemical and pharmacological aspects of capsaicin, Molecules 16 (2011) 1253–1270, https://doi.org/10.3390/molecules16021253.
[40] L. Zhang, J. Xu, Y. Tang, J. Hou, L. Yu, C. Gao, A novel long-lasting antifouling membrane modified with bifunctional capsaicin-mimic moieties via in situ polymerization for efficient water purification, J. Mater. Chem. A 4 (2016) 10352–10362, https://doi.org/10.1039/C6TA03205B.
[41] L. Zhang, C. Shan, X. Jiang, X. Li, L. Yu, High hydrophilic antifouling membrane modified with capsaicin-mimic moieties via microwave assistance (MWA) for efficient water purification, Chem. Eng. J. 338 (2018) 688–699, https://doi.org/10.1016/j.cej.2018.01.053.
[42] H. Zhang, Y. Li, S. Tian, X. Qi, J. Yang, Q. Li, C. Lin, J. Zhang, L. Zhang, A switchable zwitterionic ester and capsaicin copolymer for multifunctional marine antibiofouling coating, Chem. Eng. J. 436 (2022), 135072, https://doi.org/10.1016/j.cej.2022.135072.
[43] X. Hao, S. Chen, D. Qin, M. Zhang, W. Li, J. Fan, C. Wang, M. Dong, J. Zhang, F. Cheng, Z. Guo, Antifouling and antibacterial behaviors of capsaicin-based pH responsive smart coatings in marine environments, Mater. Sci. Eng. C 108 (2020), 110361, https://doi.org/10.1016/j.msec.2019.110361.
[44] S. Wu, Calculation of interfacial tension in polymer systems, J. Polym. Sci. Part C Polym. Symp. 34 (1971) 19–30, https://doi.org/10.1002/polc.5070340105.
[45] H. Ng, Effect of decreasing growth temperature on cell yield of Escherichia coli, J. Bacteriol. 98 (1969) 232–237, https://doi.org/10.1128/jb.98.1.232-237.1969.
[46] R. Tomičić, Z. Tomičić, N. Thaler, M. Humar, P. Raspor, Factors influencing adhesion of bacteria Escherichia coli, Pseudomonas aeruginosa, Staphylococcus aureus and yeast Pichia membranifaciens to wooden surfaces, Wood Sci. Technol. 54 (2020) 1663–1676, https://doi.org/10.1007/s00226-020-01222-0.
[47] Y.C. Jung, B. Bhushan, Wetting behavior of water and oil droplets in three-phase interfaces for hydrophobicity/philicity and oleophobicity/philicity, Langmuir 25 (2009) 14165–14173, https://doi.org/10.1021/la901906h.
[48] S. Xiao, X. Hao, Y. Yang, L. Li, N. He, H. Li, Feasible fabrication of a wear-resistant hydrophobic surface, Appl. Surf. Sci. 463 (2019) 923–930, https://doi.org/10.1016/j.apsusc.2018.09.030.
[49] E. Martinelli, I. Del Moro, G. Galli, M. Barbaglia, C. Bibbiani, E. Mennillo, M. Oliva, C. Pretti, D. Antonioli, M. Laus, Photopolymerized network polysiloxane films with dangling hydrophilic/hydrophobic chains for the biofouling release of invasive marine serpulid ficopomatus enigmaticus, ACS Appl. Mater. Interfaces 7 (2015) 8293–8301, https://doi.org/10.1021/acsami.5b01522.
[50] N. Wang, Q. Wang, S. Xu, L. Qu, Z. Shi, Robust superhydrophobic wood surfaces with mechanical durability, Colloids Surf. A 608 (2021), 125624, https://doi.org/10.1016/j.colsurfa.2020.125624.
[51] K. Zhu, J. Zhang, H. Zhang, H. Tan, W. Zhang, Y. Liu, H. Zhang, Q. Zhang, Fabrication of durable superhydrophobic coatings based on a novel branched fluorinated epoxy, Chem. Eng. J. 351 (2018) 569–578, https://doi.org/10.1016/j.cej.2018.06.116.
[52] Ç. Koşak Söz, S. Trosien, M. Biesalski, Superhydrophobic hybrid paper sheets with Janus-type wettability, ACS Appl. Mater. Interfaces 10 (2018) 37478–37488, https://doi.org/10.1021/acsami.8b12116.
[53] Y. Zou, K. Lu, Y. Lin, Y. Wu, Y. Wang, L. Li, C. Huang, Y. Zhang, J.L. Brash, H. Chen, Q. Yu, Dual-functional surfaces based on an antifouling polymer and a natural antibiofilm molecule: prevention of biofilm formation without using biocides, ACS Appl. Mater. Interfaces 13 (2021) 45191–45200, https://doi.org/10.1021/acsami.1c10747.
[54] Y. Si, Z. Dong, L. Jiang, Bioinspired designs of superhydrophobic and superhydrophilic materials, ACS Cent. Sci. 4 (2018) 1102–1112, https://doi.org/10.1021/acscentsci.8b00504.
[55] X. Wang, J. Yang, Z. Liu, X. Jiang, L. Yu, Antifouling property of Cu2O-free self-polishing antifouling coatings based on amide derivatives inspired by capsaicin, Langmuir 38 (2022) 10244–10255, https://doi.org/10.1021/acs.langmuir.2c01503.
[56] B.O.M. Oyedemi, E.M. Kotsia, P.D. Stapleton, S. Gibbons, Capsaicin and gingerol analogues inhibit the growth of efflux-multidrug resistant bacteria and R-plasmids conjugal transfer, J. Ethnopharmacol. 245 (2019), 111871, https://doi.org/10.1016/j.jep.2019.111871.
[57] J. Tang, B. Liu, L. Gao, W. Wang, T. Liu, G. Su, Impacts of surface wettability and roughness of styrene-acrylic resin films on adhesion behavior of microalgae Chlorella sp, Colloids Surf. B Biointerfaces 199 (2021), 111522, https://doi.org/10.1016/j.colsurfb.2020.111522.
[58] J. Chang, X. He, Z. Yang, X. Bai, C. Yuan, Effects of chemical composition on the hydrophobicity and antifouling performance of epoxy-based self-stratifying nanocomposite coatings, Prog. Org. Coat. 167 (2022), 106827, https://doi.org/10.1016/j.porgcoat.2022.106827.
[59] J. Chang, X. He, Z. Yang, X. Bai, R.J.K. Wood, J.A. Wharton, P. Lu, C. Yuan, Surface topography effects on the wettability and antifouling performance of nano-ZnO epoxy composite coatings, Surf. Coat. Technol. 433 (2022), 128145, https://doi.org/10.1016/j.surfcoat.2022.128145.